ORCA – Online Research @ Cardiff

This is an Open Access document downloaded from ORCA, Cardiff University's institutional repository:https://orca.cardiff.ac.uk/id/eprint/119193/

This is the author’s version of a work that was submitted to / accepted for publication.

Citation for final published version:

Sarma, Plaban Jyoti, Dey Baruah, Satyajit, Logsdail, Andrew and Deka, Ramesh Chandra 2019. Hydride pinning pathway in the hydrogenation of CO2 into formic acid on dimeric tin dioxide. ChemPhysChem 20 (5) , pp. 680-686. 10.1002/cphc.201801194

Publishers page: http://dx.doi.org/10.1002/cphc.201801194

Please note:
Changes made as a result of publishing processes such as copy-editing, formatting and page numbers may not be reflected in this version. For the definitive version of this publication, please refer to the published source. You are advised to consult the publisher’s version if you wish to cite this paper.

This version is being made available in accordance with publisher policies. See http://orca.cf.ac.uk/policies.html for usage policies. Copyright and moral rights for publications made available in ORCA are retained by the copyright holders.

# Hydride Pinning Pathway in the Hydrogenation of $CO_2$ into Formic Acid on Small Tin Dioxide Clusters

Plaban Jyoti Sarma,[a] Satyajit Dey Baruah,[a] Andrew Logsdail [b] and Ramesh Chandra Deka*[a]

**Abstract:** Capture of $CO_2$, and conversion into organic feedstocks, are of increasing need as society moves to a renewable energy economy. Here, a hydride assisted selective reduction pathway is proposed for the conversion of $CO_2$ to formic acid (FA) over $SnO_2$ monomer and dimer. Our density functional theory (DFT) calculations infer the strong chemisorption of $CO_2$ on $SnO_2$ clusters by forming a carbonate structure, whereas heterolytic cleavage of $H_2$ provides a new pathway for the selective reduction of $CO_2$ to formic acid at low overpotential. Among two investigated pathways for reduction of $CO_2$ to HCOOH, the hydride pinning pathway is found promising with a unique selectivity for HCOOH. The negatively-charged hydride forms on the cluster during the dissociation of $H_2$ and facilitates the formation of formate intermediate, which determines the selectivity for FA over alternative CO and $H_2$ evolution reaction. It is confirmed that $SnO_2$ clusters exhibit different catalytic behaviour than surface equivalents, thus offering promise for future work investigating the reduction of $CO_2$ to FA via a hydride pinning pathway at low overpotential and $CO_2$ capturing.

## Introduction

$CO_2$ is a color- and odor-less gas that contributes significantly to the phenomenon of global warming. Consumption of fossil fuels and various anthropogenic sources has led to the ceaseless emission of $CO_2$ pertaining to both short and long-term threat to the mankind and all alike.[1,2] Therefore, there has been sustained academic and commercial attempts to improve current methods of conversion or trapping of this potent greenhouse gas. Conversion of $CO_2$ into valuable chemicals such as HCOOH, $CH_3OH$, CO etc. is desirable due to their individual applications.[3-6] Among them, reduction of $CO_2$ into formic acid and methanol opens the route for the storage and transportation of $H_2$, which itself is considered a fuel of the future. Hence, both HCOOH and MeOH can serve as potential liquid chemical hydrogen storage (CHS) materials.[7] Additionally, HCOOH exists as a liquid at room temperature and can be used in a direct formic acid fuel cell.[8] Apart from that, HCOOH would prove to be more beneficial compared to other organic feedstocks due to nontoxic nature as well as ease in transportability. However, the conversion process which is critical because of its thermodynamic stability (C=O bond energy ~533 kJ/mol), requires a suitable catalyst that can bring about the activation of $CO_2$.[9] There are several possible methods by which $CO_2$ reduction can be performed, such as catalytic hydrogenation; complex metal hydrides, electrochemical reduction, photocatalysis and biological reduction. Among these methods, electro- and photo-chemical reduction of $CO_2$ to HCOOH are promising because of their high efficiency, product selectivity and lower production cost.[10-12]

Recently, Sn-based electrodes have gained popularity as a suitable catalyst because of their low toxicity and price for large-scale application.[13,14] Tin electrodes show relatively high overpotential resulting from the higher Tafel slope value (254 mV $dec^{-1}$) for the $H_2$ evolution reaction, a major competing reaction with the HCOOH formation, making the catalyst more selective towards the reduction of $CO_2$ to FA.[15] Like other non-noble metal electrodes, Sn electrodes also undergo corrosion and degradation, which leads to the deactivation of the catalyst,[16] but the effect tends to be good for Sn because the oxide layer is also catalytically active for the $CO_2$ reduction. Chen and Kanan have studied the importance of the oxide layer in the mechanism and reported that catalytic activity in presence of the oxide layer is proportional to the reduction efficiency.[17]

Numerous experimental studies have focused on the selective $CO_2$ electroreduction to formic acid using tin dioxide nanoparticles.[18-20] Meyer and co-workers investigated that by controlling nanoparticle size, a high current density of >10 $mA/cm^2$, corresponding to formate production, can be achieved at a lower overpotential of ~340 meV.[21] In another study, Kumar et al. discussed the activity of reduced $SnO_2$ nanowires towards the selectivity for HCOOH.[22] They revealed that the nanoporous nature and high numbers of grain boundaries of the particles are major factors in the enhancement of the rate and selectivity of HCOOH production. In comparison with the experimental studies theoretical investigations on the proper mechanism of $CO_2$ reduction to formic acid over $SnO_2$ catalyst are few. In the reported literature, the mechanism is initiated by the activation of $CO_2$, where the chemisorption of $CO_2$ results in a change of structure from linear to bent. After that, successive addition of 'H' to the $CO_2$ leads to the formation of formic acid. Moreover, the transfer of 'H' to the 'C' or 'O' of the $CO_2$ will determine the selectivity for the HCOOH or CO respectively.[23] Cui et al. explained the effect of surface hydroxyls on the reduction mechanism, where they promote the formation of HCOOH as a major product.[24] All these studies are relevant to the $SnO_2$ surface, but the mechanism on small sized tin dioxide, where quantum confinement and morphology are influential, remains unknown. The controlled synthesis of ~0.5-2.5 nm $SnO_2$ quantum dots is reported by Xu et al. and studied their catalytic behaviour towards ethanol sensing. They observed that the $SnO_2$ QDs shows higher sensitivity than relatively higher sized $SnO_2$ nanowires.[25] In addition, $SnO_2$ particles are also synthesized in gas phase via detonation process where Yan and coworkers reported the lowest diameters of the particle is 1 nm.[26] Therefore, in our current study, we aim to predict the global minimum structure of $SnO_2$ and $Sn_2O_4$ clusters and investigate their catalytic behaviour towards hydrogenation of $CO_2$. We identified that the growth of the nanocluster is different from the bulk and

---

[a] Mr. Plaban Jyoti Sarma, Mr. Satyajit Dey Baruah, Prof. Ramesh Chanda Deka
Department of Chemical Sciences
Tezpur Univeresity
Napaam, Sonitpur, Assam, India-784018
E-mail: ramesh@tezu.ernet.in
[b] Dr. Andrew Logsdail
School of Chemistry
Cardiff Catalysis Institute, Cardiff University, Cardiff CF10 3AT, UK

Supporting information for this article is given via a link at the end of the document.

hence the catalytic properties are also different from bulk and the surface.

Selective $CO_2$ reduction to formic acid has also been studied on other metal clusters,[27,28] metal complexes,[29] ionic liquids,[30] transition metal surfaces,[31,32] metal-hydride[33,34] and surfaces of $In_2O_3$, $CeO_2$, ZnO etc.[12,35-37] On the Cu-hydride nanocluster, $CO_2$ reduction follows a different mechanism where $CO_2$ get activated in the influence of lattice hydride and forms formate intermediate at an overpotential of 0.32 eV.[38] This investigation paves a new way of thinking about the hydride assisted pathway for the selective reduction $CO_2$ to FA over metal oxide nanoparticles; we have built our understanding around the interaction of $CO_2$ and dissociation of $H_2$ on small $SnO_2$ monomer and dimer, and subsequently investigated a new and selective path for the conversion of $CO_2$ into formic acid.

## Results and Discussion

**Global minimum structures of $SnO_2$ and $Sn_2O_4$ cluster.**

Structures of both $SnO_2$ and $Sn_2O_4$ clusters are optimized at MN12-SX/def2TZVPP level of theory (Figure 1). For $SnO_2$ cluster only a single isomer is found whereas for $Sn_2O_4$ we are reporting three low lying configurational isomer and they are presented in Fig. S1. Both GM structures are symmetric and fall in the 'D' group. $SnO_2$ cluster provides only one binding sites (Sn-O) for the guest molecule whereas the dimeric $Sn_2O_4$ structure offers two binding sites, the terminal 'Sn-O' and the bridging 'Sn-O' site. On the basis of the information as discussed, in the next sections we describe the adsorption of $CO_2$ and dissociation of $H_2$ on both of these clusters, followed by the reduction mechanism of $CO_2$.

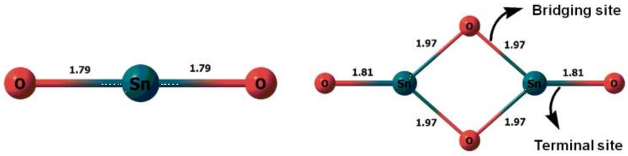

**Figure 1.** DFT optimized structure of $SnO_2$ and $Sn_2O_4$ cluster along with their symmetry point group and structural parameters.

**Adsorption of $CO_2$ on $SnO_2$ and $Sn_2O_4$ clusters.**

Optimized geometries illustrating the chemisorption behaviour of $CO_2$, on all the possible sites of both clusters, are given in Figure 2. For $SnO_2$, the $CO_2$ takes the form of carbonate structure after chemisorption, where 'O' of the $CO_2$ binds with the Sn-center and 'C' makes bond to 'O' of the cluster. The chemisorption on metal oxides of $CO_2$ has been observed to result in carbonate formation in the previous studies by Cui et al.[24] The differences in C=O bond length and $CO_2$ bond angle for the transition state and chemisorbed structures also demonstrates the activation of $CO_2$ on the $SnO_2$ cluster. The characteristic Sn-O bond length changes from 1.84 Å in transition state to 1.97 Å in the chemisorbed $SnO_2CO_2$-C and $Sn_2O_4CO_2$-C_T, while in the $Sn_2O_4CO_2$-C_B, the parent 'Sn-O' bond dissociates and forming a new 'Sn-O' bond with the 'O' of $CO_2$ maintaining a bond distance of 1.96 Å. (vdWc= van der Waals complex, C=Chemisorption, T=Terminal position, B=Bridging position). At the same time, the C-O bond elongates from 1.21 Å to 1.34-1.36 Å once $CO_2$ is bonded to the cluster. In addition, the ∠O-C-O bond angle changes from 148°-157° in TS to the range of 121°-126° in chemisorbed clusters, which is also satisfying the chemisorbed range for $CO_2$ and correlating with reported activation range of $CO_2$.[24,37] From this scenario, we can clearly see that the process of $CO_2$ activation occurs when the dimensionality of the molecule changes from linear to a planer carbonate structure.

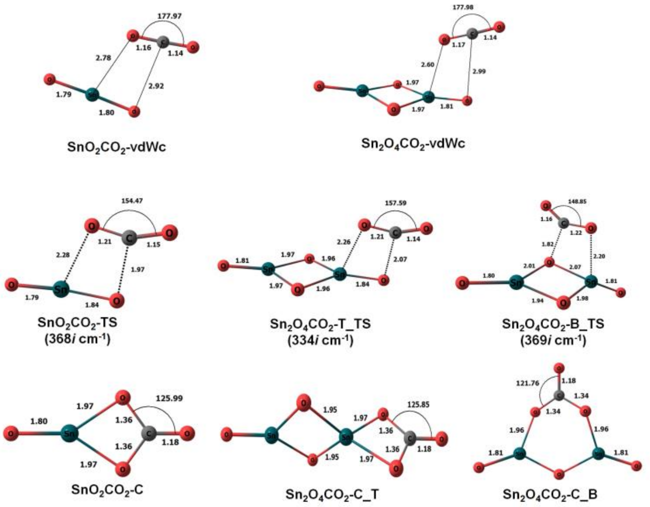

**Figure 2.** MN12-SX optimized structures of van der Waals complexes of $CO_2$ interaction as $SnO_2CO_2$-vdWc and $Sn_2O_4CO_2$-vdWc, chemisorbed $CO_2$ structures as $SnO_2CO_2$-C, $Sn_2O_4CO_2$-C_T and $Sn_2O_4CO_2$-C_B and the transition state for the interaction of $CO_2$ along with the bond length and bond angle. vdWc=van der Waals complex, C=Chemisorption, T=Terminal position, B=Bridging position, TS=Transition state.

Free energies of adsorption and activation energy for the adsorption of $CO_2$ are calculated to understand the thermodynamic feasibility of the adsorption. The adsorption energy of $SnO_2CO_2$-C is -0.26 eV (-5.98 kcal/mol) with an activation energy of 0.51 eV (11.84 kcal/mol), whereas, for $Sn_2O_4CO_2$-C_T and $Sn_2O_4CO_2$-C_B are -0.60 eV (-13.78 kcal/mol) and 0.64 eV (14.76 kcal/mol) respectively. The calculated barrier height values for $Sn_2O_4CO_2$-C_T and $Sn_2O_4CO_2$-C_B are found 0.39 eV (8.91 kcal/mol) and 0.90 eV (20.77 kcal/mol). These analyses reveal that in both clusters, the terminal position is the suitable site for the adsorption of $CO_2$ whereas the bridging site is not preferable in $Sn_2O_4$, as a substantial energy of 0.64 eV is required.

**Dissociation of $H_2$ on $SnO_2$ and $Sn_2O_4$ clusters.**

Like $CO_2$ adsorption, $H_2$ finds one active site on $SnO_2$ cluster and two (terminal 'Sn-O' and bridging 'Sn-O') sites for $Sn_2O_4$ cluster for dissociation. The clusters with dissociated $H_2$ are shown in Figure 3.

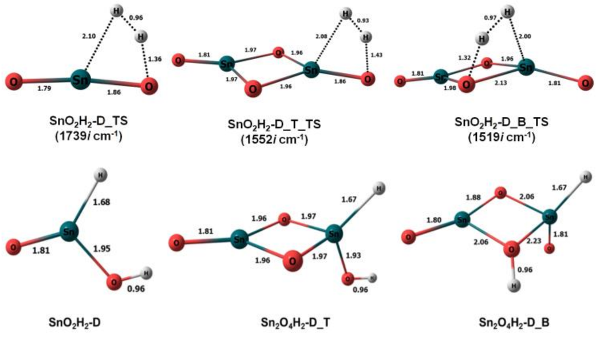

**Figure 3.** Optimized figures of $H_2$ dissociated clusters along with transition state structures at MN12-SX/def2TZVPP level of theory. (D=Dissociation, T=Terminal and B=bridging).

$H_2$ dissociation is thermodynamically favourable on both clusters, which is assessed from free energy of dissociation given in Table 1. Along with the dissociated cluster, we are presenting the transition state for the $H_2$ dissociation on both the clusters. In the monomer the barrier height is calculated 1.48 eV (34.158 kcal/mol) whereas, in dimeric cluster, two transition states are simulated to understand the dissociation nature in the terminal and bridging 'Sn-O' site. It is noteworthy to mention that although the barrier height corresponding to the $H_2$ dissociation in bridging 'Sn-O' site is more than in the terminal Sn-O site (table 1) but the elongation of 'H-H' bond length is more (0.97 Å) in $Sn_2O_4$-D_B_TS than the other two transition states. Therefore, it can be understood that even though the kinetic barrier is little more in $Sn_2O_4$-D_B_TS than $Sn_2O_4$-D_T_TS but the dissociation is predominant in the bridged position. Besides, in the TS ($Sn_2O_4$-D_B_TS), along with the elongation of H-H bond, the bridging 'Sn-O' bond also get elongated to 2.13 Å from 1.97 Å in the free $Sn_2O_4$ which is a consequence of the substantial activation energy found in $Sn_2O_4$-D_B_TS. In the dissociated clusters the formed 'Sn-H' bond lengths are 1.68 Å and 1.67 Å in the $SnO_2$ and $Sn_2O_4$ cluster respectively, while, the newly formed O-H bonds are found equal in length in all dissociated sites and that is 0.96Å. To verify the formation of hydride in each cluster, we have calculated Bader charge of each atom in the chemisorbed structure (Table 1). Bader charges of 'H' in $SnO_2H_2$-D, $Sn_2O_4H_2$-D_T and $Sn_2O_4H_2$-D_B are -0.280, -0.276 and -0.270 e respectively, indicating a gain in electron density. At this point, it is important to describe the structures of the dissociated clusters, since; the reaction mechanism of $CO_2$ reduction is dependent on the position of the 'H' atoms. $SnO_2H_2$-D is planar with the O-H hydrogen pointing out of the plane. In both $Sn_2O_4H_2$-D_T and $Sn_2O_4H_2$-D_B, the Sn-center takes a distorted tetrahedral arrangement. The analysis of ∠O-Sn-H bond angles is calculated: for $Sn_2O_4H_2$-D_T, the ∠O-Sn-H angle, with respect to the bridging O atoms, is ~120 °, whereas in $Sn_2O_4H_2$-D_B the angles are nearer to ~100 ° (Figure S2). This indicates the axial orientation of the hydride in $Sn_2O_4H_2$-D_B. Another effect associated with the structure of $Sn_2O_4H_2$-D_B, that after dissociation the Sn-O(-H) bond length increases to 2.23 Å, as a result of which the hydride tends to orient to axial position with respect to 'Sn'. To confirm our understanding of the bonding of Sn with hydride, we have also plotted a projected density of states (PDOS) for the atoms involved in 'Sn-H' bond (Supporting Information, Figure S2). The PDOS shows stronger interaction of '5s' and '5p' orbitals of Sn with the H '1s' in $Sn_2O_4H_2$-D_T than in $Sn_2O_4H_2$-D_B. This assessment suggests that the Sn 5s orbitals are involved in the bonding of 'Sn-H' in $Sn_2O_4H_2$-D_T, as is also reflected by the larger ∠O-Sn-H bond angle (typically 120 ° for $sp^2$ hybridized orbital).

**Table 1.** Free energy of dissociation of $H_2$ on $SnO_2$ clusters at 298 K. Also given are the Bader charges of reacting atoms on all the sites of the clusters (D=Dissociation, T=Terminal and B=bridging).

| Properties | Bond types | Atoms | $SnO_2H_2$-D | $Sn_2O_4H_2$-D_T | $Sn_2O_4H_2$-D_B |
|---|---|---|---|---|---|
| Free energy of Dissociation in eV (kcal/mol) | | | -1.26<br>(-29.15) | -2.04<br>(-46.98) | -0.64<br>(-14.85) |
| Activation energy eV (kcal/mol) | | | 1.48<br>(34.18) | 1.24<br>(28.79) | 1.52<br>(35.10) |
| Bader charge of characteristic atoms \|e\| | (Sn-)H | Sn | 1.921 | 2.162 | 2.010 |
| | | H | -0.280 | -0.276 | -0.270 |
| | (O-)H | O | -1.249 | -1.257 | -1.340 |
| | | H | 0.634 | 0.641 | 0.672 |

**Mechanisms for $CO_2$ reduction**

We have investigated two pathways for the reduction of $CO_2$ on $SnO_2$ clusters (Table 2):

- Case I: The formation of formic acid (FA) in a concerted process, where $H_2$ comes from the gas phase and dissociates on the terminal C=O bond to form FA. Both $SnO_2CO_2$-C and $Sn_2O_4CO_2$-C_T are eligible for this mechanism, as adsorption of $CO_2$ on both clusters is thermodynamically favourable.
- Case II (Hydride Pinning pathway): The step-wise formation of FA via a formate intermediate. Due to the presence of extra Sn-center in the $Sn_2O_4$ cluster, this mechanism is only considered for the $Sn_2O_4$ cluster: In the first step, the 'O' of $CO_2$ binds to a suitable Sn binding-site and simultaneously the 'C' is taking the hydride from the cluster. Then, in the second step, the remaining H is transferred to the unbound O of the adsorbed HCOO* intermediate.

**Table 2.** Two different Cases that are considered for the formation of HCOOH from reduction of $CO_2$

| Pathway | Reaction |
|---|---|
| HCOOH formation via case I | $CO_2^* + H_2 \rightarrow HCOOH^*$ |
| HCOOH formation via case II | $CO_2 + H^* \rightarrow HCOO^*$<br>$HCOO^* + H^* \rightarrow HCOOH$ |

**$CO_2$ reduction to HCOOH on both $SnO_2$ and $Sn_2O_4$ cluster via Case I.**

This mechanism is effectively the direct hydrogenation of $CO_2$ to Formic acid, with $H_2$ dissociation taking place on the unbound C=O bond of $SnO_2CO_2$-C and $Sn_2O_4CO_2$-C_T. Since the formation of HCOOH does not involve any intermediate, the whole reaction has only one transition state, represented as TS1 and TS2 in Figure 4. These TSs correspond to the formation of HCOOH on $SnO_2$ and $Sn_2O_4$ clusters and are characterized by the presence of one imaginary frequency of 2246*i* $cm^{-1}$ and 2249*i* $cm^{-1}$.

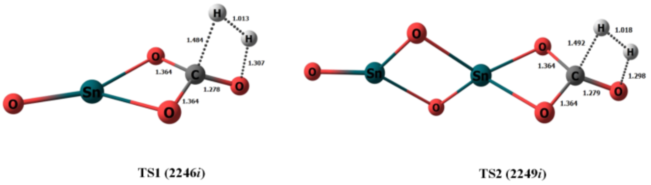

TS1 (2246*i*)

TS2 (2249*i*)

**Figure 4.** Transition states TS1 and TS2 for the formation of HCOOH via case I.

In the transition state, the H••H bond is elongated from 0.74 Å to 1.01Å when adsorbed on the cluster. The bond distance of newly formed C••H bonds are 1.48 Å and 1.49 Å, whereas the O••H bonds are 1.30Å and 1.29 Å in TS1 and TS2 respectively. The free energy profile diagram presented in Figures 5, signify the case I pathway for the $CO_2$ reduction on $SnO_2$ and $Sn_2O_4$ cluster respectively.

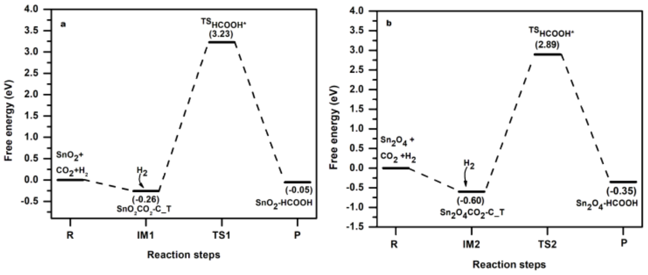

**Figure 5:** Free energy profile for $CO_2$ reduction on $SnO_2$ (a) and $Sn_2O_4$ (b) clusters via Case I, as calculated at MN12-SX/def2tzvpp level of theory.

From Figure 5, we can see that the free energies of activation for TS1 and TS2 are 3.492 eV (80.54 kcal/mol) and 3.490 eV (80.50 kcal/mol), respectively, which is substantial. The difference in energy between the TSs is only 0.002 eV, so the energetic profiles are very similar for both of the clusters towards catalytic formation of HCOOH via Case I. Clearly, the major drawback of this mechanism is the large energy barrier, which would lead to kinetic infeasibility for the reaction. The high activation energy is attributed to the strong binding of $CO_2$ with the clusters; additionally, for the final product, the formed HCOOH binds favourably in a tetrahedral manner with the Sn-center in the cluster, rather than leaving the catalytic site and this could deactivate the catalyst. Thus, we can conclude that $CO_2$ reduction is infeasible via this mechanism, though an alternative conclusion is that the strong binding of $CO_2$ with the cluster offers promise for application as a carbon dioxide trapping material, which is very important part of $CO_2$ mitigation.

### $CO_2$ reduction to HCOOH on $Sn_2O_4$ cluster via Case II.

We have already mentioned while introducing the Case II that the 'Hydride pinning pathway' is only feasible for the $Sn_2O_4$ cluster. Thus, the first question to address is why the monomeric cluster is not a suitable candidate for this mechanism: the lack of a second Sn-center in the cluster limits HCOO formation and hence formic acid. As a result, rather forming a formate intermediate, carbonate structure is reformed via the chemisorption of $CO_2$ (Figure S3). This outcome is due to the unsaturated nature of 'Sn' in $SnO_2$ cluster.

In the hydride pinning step over $Sn_2O_4$, the HCOO* intermediate forms as a result of the transfer of hydride from the $Sn_2O_4$ cluster to the 'C' of $CO_2$ and simultaneously the 'O' of $CO_2$ binds with another Sn-center in the cluster. Before unraveling the in-depth detailed mechanistic pathway, it is worth mentioning that, even though $H_2$ dissociates heterolytically on both terminal and bridging Sn-O sites of the $Sn_2O_4$ cluster, to give $Sn_2O_4H_2$-D_T and $Sn_2O_4H_2$-D_B, the hydride pinning pathway proceeds only via the formation of $Sn_2O_4H_2$-D_B. The reason for this selectivity is attributed to the hydride orientation towards the $CO_2$ binding site, whereas the hydride of $Sn_2O_4H_2$-D_T is oriented away from the $CO_2$ binding site. These observations strongly suggest that the mechanism proceeds via $Sn_2O_4H_2$-D_B, followed by the hydride pinning step.

A free energy diagram for the overall reaction mechanism is presented in Figure 6. The favorable interaction at the pinning step (IM3 → IM4$^{/}$) is mainly attributed to the attraction of positively charged 'C' of $CO_2$ towards the negatively charged hydride. In this step, $CO_2$ comes from the gas phase and proceed through a transition state TS3 (574*i* $cm^{-1}$) with an activation energy of 1.15eV (26.51 kcal/mol) to take up the hydride form the 'Sn'. In TS3, the C••H and Sn••O distances are 1.48 Å and 2.26 Å, respectively, whereas the bond length that corresponds to the breaking of Sn••H bond is 1.81 Å. The formed HCOO* intermediate (IM4) remains adsorbed on the cluster via one 'O' of $CO_2$, with the unbound 'O' of the HCOO* oriented away from the cluster, however a spontaneous structural transformation occurs with a free energy change (ΔG) of -0.52 eV (-11.99 kcal/mol) which gives IM4$^{/}$ where, the 'O=C-H' group flips around the Sn-O single bond. Finally, IM4$^{/}$ has the (C-)H pointed upward and the unbound 'O' makes a weak stabilizing interaction with the Sn maintaining 2.38 Å of bond distance. A major advantage of this structural change is that the weakly bonded 'O' is now nearer to the second hydrogen, which is bonded to one of the bridging 'O' of the cluster. In the last step, the remaining 'H' is transferred to the 'O' and forms HCOOH via a transition state TS4 (1003*i* $cm^{-1}$), with an activation energy of 0.33eV (7.63 kcal/mol). In the same step the HCOOH also desorbs from the catalytic site, thus facilitating the regeneration of the catalyst to undergo $H_2$ dissociation and repeat the catalytic cycle.

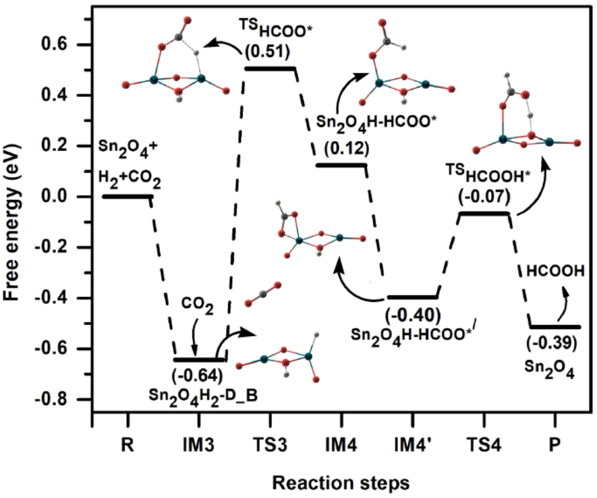

**Figure 6.** Complete potential energy surface diagram for hydride pinning pathway (Case II) for $CO_2$ reduction calculated at MN12-SX/def2tzvpp level of theory.

After analysis of the free energy diagram, we can clearly state that the pinning step (hydride transfer) is the rate determining step (RDS) of the reaction. Moreover, in this RDS, the ΔG difference between the IM3 and IM4/ is only 0.24 eV, which is an indicator of the necessary overpotential for HCOOH production vs RHE. Previous experimental studies report the overpotential for HCOOH formation on $SnO_2$ nanoparticles as 0.34-0.35 eV[21,22] and theoretical value reported on copper hydride ($Cu_{32}H_{20}L_{12}$, $L=S_2PH_2$) nanocluster is 0.32 eV.[38] The simulation models and experimental catalysts differ in size but the consistency between results confirms the validity of our approach; furthermore, the subtle differences between experimental and calculated overpotential suggest opportunities to tune the size of the nanoparticle specifically to aid the reduction mechanism of $CO_2$ to formic acid. The overall reaction cycle for the hydride pinning pathway is shown in Figure 7.

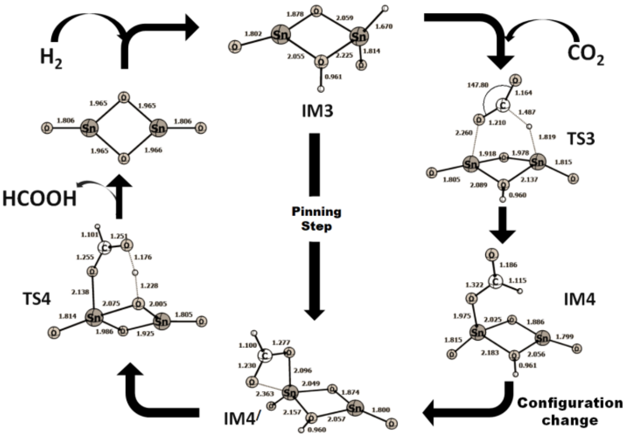

**Figure 7.** Total reaction Cycle of HCOOH formation from $CO_2$ via hydride pinning pathway.

Thus far, we have discussed the formation of formic acid via the hydride mechanism, but there exist other competing processes such as $H_2$ evolution reaction and CO formation reactions along with the HCOOH formation. To consider these side reactions, we have studied the $H_2$ recombination reaction using the $Sn_2O_4H_2$-D_B structure as a source for $H_2$ evolution. The $\Delta G^{\ddagger}$ and ΔG for the $H_2$ recombination reaction are found to be 2.17 eV and 0.64 eV, respectively. A free energy diagram, shown in Figure S4 is the comparison between the formate formation and $H_2$ recombination reactions, alongside the structure of transition state corresponding to the $H_2$ recombination. Therefore, $H_2$ recombination will not hinder the HCOOH formation. On the other hand, formation of CO along with $H_2O$ will be inevitable if the hydride is transferred to the 'O' of $CO_2$ instead of 'C'. We have substantiated two factors to describe the inhibition of CO formation: 1) the hydride lacks adequate ability to bond with the 'O' of $CO_2$ as both are negatively charged i.e. coulombic repulsion; 2) there is an absence of a binding site for a COOH intermediate. To confirm this, we have modelled a structure where 'O' of $CO_2$ takes the 'H' from 'Sn' and forms COOH* intermediate (SI, Figure S5). We have demonstrated that, after formation of a COOH* intermediate, reorientation is necessary with adsorption to the cluster via the 'C' atom. This is also observed in previous literature by Tang et al.[38] but the bridging oxygens of our cluster are coordinately saturated, so a carbonate structure will be formed if 'C' binds to the terminal 'O' of the cluster, rather picking up the 'H' from the Sn-center to form the COOH intermediate.

## Conclusions

In summary, structures and catalytic activity of $SnO_2$ atomic clusters are investigated towards the reduction of $CO_2$ using DFT method. Adsorption of $CO_2$ on the clusters results in a stable carbonate structure whereas dissociation of $H_2$ opens a hydride assisted channel for reduction of $CO_2$ to HCOOH. The stepwise hydride pinning pathway (Case II) is auspicious in determining the selectivity for HCOOH over case I. After the formation of HCOOH, desorption of the product occurs spontaneously and the catalyst active site is regenerated. Using the computational hydrogen electrode (CHE) model, our results suggest the required overpotential for HCOOH formation is 0.24 eV. The low overpotential is a consequence of having extra Sn-center in the dimer, which plays a crucial role in stabilizing the HCOO* intermediate. Along with the HCOOH formation, $H_2$ recombination is also studied and a large activation barrier of 2.12 eV confirms that $H_2$ evolution is not a major issue in the hydride pinning mechanism. Moreover, the presence of hydride in the cluster inhibits the formation of COOH* intermediate and therefore, CO formation reaction is not a topic of concern in $CO_2$ reduction via hydride assisted pathway, as justified via coordination and electrostatic arguments. In the final touch, we put forward two benefits of using $SnO_2$ nanoclusters: firstly, both clusters are notable at $CO_2$ trapping material and, secondly, the $Sn_2O_4$ cluster serves as a tremendous catalyst with respect to reducing $CO_2$ to formic acid via the mechanism initiated by $H_2$ dissociation. These results offer a great platform for further experimental studies to develop our understanding of $CO_2$ reduction to formic acid via hydride pinning pathway.

## Computational Details

Structures, reaction energies and the detailed mechanism of $CO_2$ reduction are studied using Kohn-Sham density functional theory (DFT) as available on Gaussian 09 quantum chemistry software package.[39] Critical bond dissociation enthalpies of Sn-O, C-O, O-H, C-H, and Sn-H bonds are calculated at 22 tested methods employing density fitting triple-ξ def2TZVPP basis set [40,41] as shown in Table S1. The best outcome of the initial analysis is the range-separated hybrid meta-NGA (non-separable gradient approximation) MN12-SX functional [42] in describing bond dissociation enthalpies of the bonds close to experimental data. The accuracy of MN12-SX functional agrees with previous studies in predicting both structures and energies.[43,44] Along with it, the def2TZVPP basis set proves very good in minimizing the basis set superposition error (BSSE), giving errors of < 0.04 eV, thus providing results close to the DFT basis set limit.[41] Therefore, for geometry relaxation and frequency calculation, we have used MN12-SX/def2TZVPP level employing ultrafine integration grid. All reported adsorption and dissociation energies in the manuscript are also corrected appropriately for BSSE. Genetic algorithm is used for global optimization of $SnO_2$ and $Sn_2O_4$ clusters.[45] Presence of only one imaginary frequency in the vibrational spectra confirms identified transition states, consistent with the eigenvector along the reaction coordinate, whereas, for the reactant, intermediates, and products, no imaginary frequency is observed, confirming that they are true minima. Gibbs free energy change (ΔG), at 1 atm pressure and 298K temperature are calculated for each step in the reaction mechanisms by referring to the free energy difference between the final and initial states; the calculations for the free energy of adsorption and dissociation at room temperature have been analyzed in a similar manner. The free energy of activation ($\Delta G^{\ddagger}$) of the transition states are calculated by measuring the free energy change of transition state with respect to the initial state. To gain a more detailed insight into the electronic charge distribution, Bader charge analysis is done using AIMALL software package, verifying the formation of hydride on the $H_2$ dissociation step.[46] As the product (HCOOH) is formed in liquid phase, a correction to the free energy for HCOOH is included in calculating the reaction energetics, as shown in Supporting Information (Section 1). The computational hydrogen electrode (CHE) model is used to correlate the reaction free energy change with the electrochemical potential, with respect to the transfer of hydrogen from the catalyst to $CO_2$ while forming the HCOO* intermediate. At 1 atm, the CHE assumes that the protons and electrons are at equilibrium with the gas phase hydrogen ($H^+ + e^- \rightarrow 1/2H_2$) at potential 0V vs RHE for all pH and all temperature.[47]

## Acknowledgements

The authors are thankful to Science & Engineering Research Board (SERB) (EMR/2016/003195), Department of Science and Technology (DST) (No: DST/INSPIRE Fellowship/[IF160658]) New Delhi, India, and Tezpur university for financial support. Authors acknowledge UK-India Education and Research Initiative (UKIERI) for research fund (Grant No. DST/INT/UK/P-35/2012) to carry out collaborative research work. The authors gratefully acknowledge the support of Prof. C. R. A. Catlow, FRS.

**Keywords:** $SnO_2$ and $Sn_2O_4$ cluster, MN12-SX Functional, $CO_2$ reduction, Formic acid, Hydride Pinning Pathway.

[1] A. Stips, D. Macias, C. Coughlan, E. Garcia-Gorriz, X. S. Liang, *Sci. Rep.* **2016**, *6*, 21691−21699.

[2] J. Klankermayer, S. Wesselbaum, K. Beydoun, W. Leitner, *Angew. Chemie - Int. Ed.* **2016**, *55*, 7296–7343.

[3] S. Roy, B. Sharma, J. Pécaut, P. Simon, M. Fontecave, P. D. Tran, E. Derat, V. Artero, *J. Am. Chem. Soc.* **2017**, *139*, 3685−3696.

[4] A. Álvarez, A. Bansode, A. Urakawa, A. V. Bavykina, T. A. Wezendonk, M. Makkee, J. Gascon, F. Kapteijn, *Chem. Rev.* **2017**, *117,* 9804–9838.

[5] Q. Li, J. Fu, W. Zhu, Z. Chen, B. Shen, L. Wu, Z. Xi, T. Wang, G. Lu, J. Zhu, S. Sun, *J. Am. Chem. Soc.* **2017***, 139*, 4290–4293.

[6] D. Ballivet-Tkatchenko, S. Chambrey, R. Keiski, R. Ligabue, L. Plasseraud, P. Richard, H. Turunen, *Catalysis Today*, **2006**, *115*, 80-87.

[7] K. Sordakis, C. Tang, L. K. Vogt, H. Junge, P. J. Dyson, M. Beller, G. Laurenczy, *Chem. Rev.* **2018,** *118*, 372–433.

[8] X. Yu, P. G. Pickup, *Journal of Power Sources*. **2008**, 182, 124−132.

[9] A. Bhowmik, T. Vegge, H. A. Hansen, *Chem. Sus. Chem.* **2016***, 9,* 3230–3243.

[10] J. Wu, Y. Huang, W. Ye, Y. Li, *Adv. Sci.* **2017**, *4*, 1–29.

[11] A. C. Khezri, M. Fisher, J. Pumera, *Mater. Chem. A* **2017**, *5*, 8230–8246.

[12] Y. Tamaki, K. Koike, O. Ishitani, *Chem. Sci.* **2015,** *6*, 7213–7221.

[13] J. Wu, F. G. Risalvato, S. Ma, X. D. Zhou, *J. Mater. Chem. A* **2014***, 2*, 1647–1651.

[14] J. Medina-Ramos, R. C. Pupillo, T. P. Keane, J. L. Dimeglio, J. Rosenthal, *J. Am. Chem. Soc.* **2015,** *137*, 5021–5027.

[15] E. Irtem, T. Andreu, A. Parra, M. D. Hernández-Alonso, S. García-Rodríguez, J. M. Riesco-García, G. Penelas-Pérez, J. R. Morante, *J. Mater. Chem. A* **2016**, *4*, 13582–13588.

[16] G. S. Frankel, A. Agarwal, N. Sridhar, *Electrochim. Acta* **2014***, 133*, 188–196.

[17] Y. Chen, M. W. Kanan, *J. Am. Chem. Soc.* **2012***, 134*, 1986–1989.

[18] S. Lee, J. D. Ocon, Y. Son, J. Lee, *J. Phys. Chem. C* **2015***, 119*, 4884–4890.

[19] W. Lee, N. H. Cho, K. D. Yang, K. T. Nam, *Chem. Electro. Chem.* **2017***, 4*, 2130–2136.

[20] K. R. Rao, S. Pishgar, J. Strain, B. Kumar, V. Atla, S. Kumari, J. M. Spurgeon, *J. Mater. Chem. A* **2018***, 6*, 1736–1742.

[21] S. Zhang, P. Kang, T. J. Meyer, *J. Am. Chem. Soc.* **2014***, 136*, 1734–1737.

[22] B. Kumar, V. Atla, J. P. Brian, S. Kumari, T. Q. Nguyen, M. Sunkara, J. M. Spurgeon, *Angew. Chemie - Int. Ed.* **2017***, 56*, 3645–3649.

[23] K. Saravanan, Y. Basdogan, J. Dean, J. A. Keith, *J. Mater. Chem. A* **2017***, 5*, 11756–11763.

[24] Cui, J. Han, X. Zhu, X. Liu, H. Wang, D. Mei, Q. Ge, *J. Catal.* **2016***, 343,* 257–265.

[25] X. Xu, J. Zhuang, X. Wang, *J. Am. Chem. Sos*. **2008**, *130*, 12527-12535.

[26] Y. Honghao, W. Linsong, L. Xiaojie, W. Xiaohong, *Rare Metal Mat. Eng.* **2013**, *42*, 1325-1327.

[27] Cai, D. Gao, H. Zhou, G. Wang, T. He, H. Gong, S. Miao, F. Yang, J. Wang and X. Bao, *Chem. Sci.,* **2017***, 8,* 2569–2573.

[28] C. Liu, H. He, P. Zapol, L. A. Curtiss, *Phys. Chem. Chem. Phys.* **2014***, 16,* 26584–26599.

[29] T. N. Huan, P. Simon, A. Benayad, L. Guetaz, V. Artero, M. Fontecave, *Chem. Eur. J*. **2016**, *22*, 14029 – 14035.

[30] T. N. Huan, P. Simon, G. Rousse, I. Genois, V. Artero, M. Fontecave, *Chem. Sci.* **2017***, 8*, 742–747.

[31] W. Lin, K. M. Stocker, G. C. Schatz, *J. Am. Chem. Soc.* **2017** *139*, 4663–4666.

[32] C. Liu, T. R. Cundari, A. K. Wilson, *J. Phys. Chem. C* **2012***, 116*, 5681–5688.

[33] W. Sun, C. Qian, L. He, K. K. Ghuman, A. P. Y. Wong, J. Jia, A. A. Jelle, P. G. O'Brien, L. M. Reyes, T. E. Wood, A. S. Helmy, C. A. Mims, C. V. Singh, G. A. Ozin, *Nat. Commun.* **2016***, 7*, 12553–12561.

[34] K. M. Waldie, A. L. Ostericher, M. H. Reineke, A. F. Sasayama, C. P. Kubiak*, ACS Catal.* **2018***, 8*, 1313–1324.

[35] D. Gao, Y. Zhang, Z. Zhou, F. Cai, X. Zhao, W. Huang, Y. Li, J. Zhu, P. Liu, F. Yang, G. Wang, X. Bao *J. Am. Chem. Soc.* **2017***, 139*, 5652–5655.

[36] X. Zhao, X. Huang, X. Wang, *J.* Wang, *Mater. Chem. A* **2017***, 5*, 21625–21649.

[37] X. Lu, W. Wang, S. Wei, C. Guo, Y. Shao, M. Zhang, Z. Deng, H. Zhu, W. Guo, *RSC Adv.* **2015***, 5,* 97528–97535.

[38] Q. Tang, Y. Lee, D. Y. Li, W. Choi, C. W. Liu, D. Lee, D. E. Jiang, *J. Am. Chem. Soc.* **2017***, 139*, 9728–9736.

[39] M. J. Frisch, G. W. Trucks, H. B. Schlegel, G. E. Scuseria, M. A. Robb, J. R. Cheeseman, G. Scalmani, V. Barone, B. Mennucci, G. A. Petersson, H. Nakatsuji, M. Caricato, X. Li, H. P. Hratchian, A. F. Izmaylov, J. Bloino, G. Zheng, J. L. Sonnenberg, M. Hada, M. Ehara, K. Toyota, R. Fukuda, J. Hasegawa, M. Ishida, T. Nakajima, Y. Honda, O. Kitao, H. Nakai, T. Vreven, J. A. Montgomery, Jr., J. E. Peralta, F. Ogliaro, M. Bearpark, J. J. Heyd, E. Brothers, K. N. Kudin, V. N. Staroverov, R. Kobayashi, J. Normand, K. Raghavachari, A. Rendell, J. C. Burant, S. S. Iyengar, J. Tomasi, M. Cossi, N. Rega, J. M. Millam, M. Klene, J. E. Knox, J. B. Cross, V. Bakken, C. Adamo, J. Jaramillo, R. Gomperts, R. E. Stratmann, O. Yazyev, A. J. Austin, R. Cammi, C. Pomelli, J. W. Ochterski, R. L. Martin, K. Morokuma, V. G. Zakrzewski, G. A. Voth, P. Salvador, J. J. Dannenberg, S. Dapprich, A. D. Daniels, Ö. Farkas, J. B. Foresman, J. V. Ortiz, J. Cioslowski, and D. J. Fox, Gaussian09 Revision D.01, Gaussian Inc. Wallingford CT. **2010**.

[40] F. Weigend, *Phys. Chem. Chem. Phys.* **2006***, 8,* 1057–1065.

[41] F. Weigend, R. Ahlrichs, *Phys. Chem. Chem. Phys.* **2005***, 7,* 3297–3305.

[42] R. Peverati, D. G. Truhlar, *Phys. Chem. Chem. Phys.* **2012***, 14*, 16187–16191.

[43] J. Frau, D. Glossman-Mitnik, *Theor. Chem. Acc.* **2018**, *137*, 67–76.

[44] S. Paranthaman, J. Moon, J. Kim, D. E. Kim, T. K. Kim, *J. Phys. Chem. A* **2016***, 120*, 2128–2134.

[45] M. R. Farrow, Y. Chow, S. M. Woodley, *Phys. Chem. Chem. Phys.* **2014***, 16*, 21119–21134.

[46] AIMAll (Version 17.11.14), Todd A. Keith, TK Gristmill Software, Overland Park KS, USA, **2017** (aim.tk gristmill.com).

[47] J. K. Nørskov, J. Rossmeisl, A. Logadottir, L. Lindqvist, J. R. Kitchin, T. Bligaard, H. Jónsson, *J. Phys. Chem. B* **2004**, *108*, 17886–17892.

**Entry for the Table of Contents** (Please choose one layout)

## FULL PAPER

Text for Table of Contents

**Representation of different paths involved in the hydrogination of $CO_2$ to formic acid:** The modelled $Sn_2O_4$ cluster has shown a unique selectivity towards HCOOH when the mechanism proceeds via hydride assisted pathway (commiting step) over CO formation and $H_2$ recombination reactions (limiting steps).

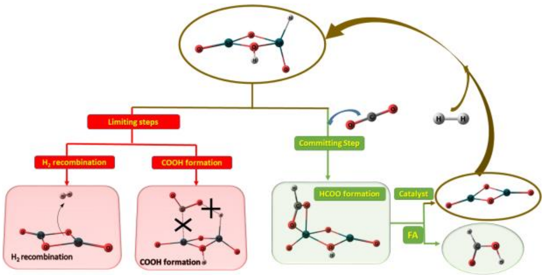
Limiting steps
Committing Step
H₂ recombination
COOH formation
H₂ recombination
COOH formation
HCOO formation
Catalyst
FA
H
H

*Plaban Jyoti Sarma, Satyajit Dey Baruah, Andrew Logsdail, Ramesh Chandra Deka**

***Page No. – Page No.***

**Hydride Pinning Pathway in the Hydrogenation of CO2 into Formic Acid on Small Tin Dioxide Clusters**